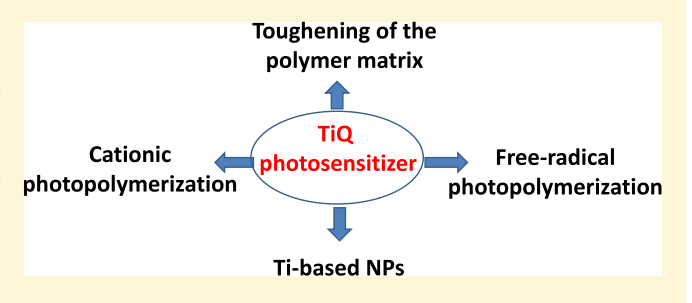
Macromolecules 2019, 52, 3716–3729

Well-Defined Titanium Complex for Free-Radical and Cationic Photopolymerizations under Visible Light and Photoinduction of Ti-**Based Nanoparticles**

Louise Breloy,[†] Vlasta Brezová,[‡] Jean-Pierre Malval,[§] Agustin Rios de Anda,[†] Julie Bourgon,[†] Takashi Kurogi, ^{||} Daniel J. Mindiola, ^{||} and Davy-Louis Versace*,[†]

Supporting Information

ABSTRACT: A quinoline-derived titanium complex (TiQ) is shown here to possess remarkable photosensitizing properties when treated with an iodonium salt (Iod) to initiate, under visible light irradiation, (i) the free-radical photopolymerization of acrylate monomer in aerated/laminate conditions, (ii) the cationic photopolymerization of epoxy monomer under air, and (iii) the in situ formation of Ti-based nanoparticles (NPs) inside coatings. The photochemical properties of the TiQ/Iod photoinitiating system have been probed by electron paramagnetic resonance, laser flash photolysis, and real-time



Fourier transform infrared spectroscopy, which provide an insight into the possible radical/cationic pathways. The microstructural properties of the photosynthesized Ti-based NPs have been investigated by bright-field conventional transmission electron microscopy and high-angle annular dark-field scanning transmission electron microscopy. The macroscopic mechanical properties of the resulting nanocomposite reveal that the generation of these Ti-based NPs in a polyacrylate/polyether blend matrix leads to an increase of mechanical resistance by toughening the matrix.

■ INTRODUCTION

The synthesis of nanocomposites under light exposure is a promising research topic, notably in dentistry. The most common approach (ex situ method) consists of a mixture of (meth)acrylate matrix, inorganic fillers, and visible light photoinitiating systems. Some examples were described for dental chemical uses. 1-10 To date, the most common photoinitiator used in dental applications has been camphorquinone, and inorganic fillers can be silane-treated inorganic fillers, silica, silanized glass fillers, or barium boroaluminosilicate glass particles. Another way to generate nanoparticles (NPs) inside polymer matrix is the in situ technique. Various metal NPs (Ag, Au, Pd, Cu, Zr, Ti, among many other metals) have been synthesized in solution or in coatings by the reduction of metal salt precursors. 11-17 Typically, this procedure involved a photoinitiator (PI) and a metal salt precursor. Under light exposure, the homolytic cleavage of PI simultaneously leads to the formation of two radicals: 18 One radical that can initiate the photopolymerization, and the other reduces the metal salt. Such a strategy has led to successful

incorporation of Ag, Au, or Cu nanoparticles in a photogenerated matrix. $^{19-30}$

The coupling of PI and metallic agent has also been declined through the use of metal-functionalized PIs such as a goldthiophene derivative, 13 an Ag-thioxanthone derivative, 28 an Agdiaminofluorene derived dye,³¹ or an Ag-phosphine derivative complex.²⁹ Most of these initiating systems have permitted the formation of polyacrylate nanocomposites upon light irradiation. However, one limitation is their sensitivity to oxygen, which is a strong inhibitor to free-radical photopolymerization. Indeed, under air, oxygen reacts with the radicals created during the initiating process to yield peroxyls ROO (1), which are not reactive toward the acrylate double bonds and cannot further initiate any polymerization reactions.

Recently, an approach to photogenerate nanocomposites by involving a bimolecular homolytic substitution reaction (S_H2

Received: December 21, 2018 Revised: April 12, 2019 Published: May 8, 2019

[†]Institut de Chimie et des Matériaux Paris-Est, Equipe Systèmes Polymères Complexes, UMR 7182, CNRS-Université Paris-Est Créteil (UPEC), 2-8 rue Henri Dunant, 94320 Thiais, France

[‡]Institute of Physical Chemistry and Chemical Physics, Faculty of Chemical and Food Technology, Slovak University of Technology in Bratislava, Radlinskeho 9, SK-812 37 Bratislava, Slovak Republic

[§]Institut de Science des Matériaux de Mulhouse, IS2M-LRC 7228, 15 rue Jean Starcky, 68057 Mulhouse, France

School of Arts and Sciences, Department of Chemistry, University of Pennsylvania, 231 S. 34 Street, Philadelphia, Pennsylvania, United States

Scheme 1. Synthetic Entry to Complex TiQ from Precursor (PNP)Ti = CH^tBu(CH₂^tBu)^a

$$(PNP)Ti \longrightarrow CH_2^tBu \longrightarrow (PNP)Ti \longrightarrow (PN$$

^aFor simplicity, the pincer ligand is shown as a caricature PNP (inset).

process) has been developed. The relative ineffective peroxyl radicals are converted into new performing radical species by using the appropriate photoinitiating system combination (PI/ metal complex). Indeed, this process has been exploited using formulations containing free-radical photoinitiators such as 2,2-dimethoxy-2-phenylacetophenone (DMPA); bis-(cyclopentadienyl)titanium dichloride³² (Cp₂TiCl₂) or bis-(cyclopentadienyl)zirconium dichloride; 33 and polyethylene glycol (400) diacrylate (PEGDA) or trimethylolpropane triacrylate (TMPTA) as a polymerized matrix. For example, we demonstrated that the addition of peroxyls to Cp₂ZrCl₂ (2) leads to the formation of cyclopentadienyl radicals (Cp[•]), which readily initiate the free-radical polymerization of TMPTA (3). The successive addition of peroxyls to putative CpZrCl₂(OOR) has been shown to be responsible for the in situ generation of Zr-based NPs (4).

$$R^{\bullet} + O_2 \rightarrow \text{peroxyls (ROO}^{\bullet})$$
 (1)

$$ROO^{\bullet} + Cp_2ZrCl_2 \rightarrow CpZrCl_2(OOR) + Cp^{\bullet}$$
 (2)

$$Cp^{\bullet} + acrylate \rightarrow polyacrylate$$
 (3)

$$ROO^{\bullet} + CpZrCl_2(OOR) \rightarrow \rightarrow Zr - based NPs (h\nu)$$
(4)

In a previous investigation, we also demonstrated that the use of titanium alkoxides,³⁴ namely, titanium isopropoxide or titanium (triethanolaminato) isopropoxide precursors, with a UV-cleavable photoinitiator (bis(2,4,6-trimethylbenzoyl)-phenylphosphineoxide, BAPO) appears to be efficient photoinitiating systems that overcome the oxygen inhibition effects in free-radical photopolymerization of TMPTA. These systems under air and upon exposure to a low-intensity UV light activation result in simultaneous formation of Ti-based NPs. More recently, the synthesis of visible-light-absorbing Ti-based NPs³⁵ in a polyether film has been demonstrated using UV light irradiation of a titanium isopropoxide/(4-methylphenyl)-[4-(2-methylpropyl) phenyl]-hexafluorophosphate (Iod) couple under air and in a cationic monomer film.

Unfortunately, one of the major drawbacks for the aforementioned investigations is the use of UV light (or UV-polychromatic emission lamps) for initiating free-radical or cationic photopolymerization. In the present paper, we report, for the first time, a novel photoinitiating system based on a titanium-derivative compound, which can absorb in the visible range, while using an iodonium salt (Iod). In this context, a new titanium-conjugated complex (PNP)TiN[$C_{18}H_{13}N$] (TiQ), obtained from the reaction of the alkylidene—alkyl complex of titanium, namely, (PNP)Ti = $CH^tBu(CH_2^tBu)$ (PNP = $N[2-P^tPr_2-4$ -methylphenyl]⁻), and 2 equiv of

quinoline (an industrial waste) under mild conditions as described in Scheme 1, was used.

Due to its low oxidation potential and high molar absorption coefficient in the close and visible range, TiQ is well adapted for the reduction of iodonium salts upon monochromatic light irradiation. Therefore, we investigate here the capability of TiQ to simultaneously promote cationic and free-radical polymerizations upon 385 and 405 nm LED exposure, when used as a photosensitizer of an iodonium salt (Iod), and the in situ formation of Ti-based NPs in a photopolymerizable acrylate and/or epoxy matrices under air. The reactivity of the TiQ/Iod photoinitiating system is first demonstrated by steady-state photolysis and real-time infrared Fourier transform spectroscopy (RT-FTIR). Finally, the proposed chemical reactions according to different atmospheric conditions (under air or oxygen-free reactions) have been investigated through electronic paramagnetic resonance (EPR) spintrapping, fluorescence, laser flash photolysis measures, as well as transmission electron microscopy (TEM) experiments. A new proposed mechanism concerning the synthesis of in situ Ti-based NPs under air and visible light irradiation has been evidenced by EPR. The impact of the photoinduced Ti-based NPs on the mechanical properties of the resulting nanocomposites has been thoroughly characterized by three-point bending tests.

EXPERIMENTAL SECTION

Materials. TiQ was prepared according to the literature.³⁶ Biphenyl, Rhodamine B (RhB, ≥95%), trimethylolpropane tris(3-mercaptopropionate) (Trithiol), benzophenone (BP), 2-isopropylthioxanthone (ITX), N-methyl diethanol amine (MDEA), bis(4-methylphenyl) iodonium hexafluorophosphate (Iod), the spin trapping agent 4-oxo-2,2,6,6-tetramethylpiperidine (TMPO), and solvents were purchased from Sigma-Aldrich and used as received without further purification. The spin trap agent, i.e., 5,5-dimethyl-1-pyrroline N-oxide (DMPO, Sigma-Aldrich), was distilled prior to the application. Monomers (3,4-epoxycyclohexane)methyl 3,4-epoxycyclohexylcarboxylate (EPOX) and trimethylolpropane triacrylate (TMPTA) were obtained from Sigma-Aldrich and Cytec, respectively, and used as received. These are reference monomers for studying the photochemical systems.

Methods. X-Band Electronic Paramagnetic Resonance (EPR) Spectroscopy. The X-band electronic paramagnetic resonance (EPR) spectroscopy experiments were carried out by means of EMXplus spectrometer (Bruker) with a high-sensitivity probe-head (Bruker) in the small quartz flat cell (WG 808-Q, Wilmad-LabGlass; optical cell length, 0.045 cm), or by an EMX spectrometer (Bruker) with the standard TE₁₀₂ (ER 4102 ST) rectangular cavity using thin-walled quartz EPR tubes (Bruker). The solutions prepared in benzene were saturated with argon. The samples were irradiated at 293 K directly in the EPR resonator using an LED source ($\lambda_{\rm max}$ = 400 nm; Bluepoint LED, Hönle UV Technology), and the EPR spectra were recorded in

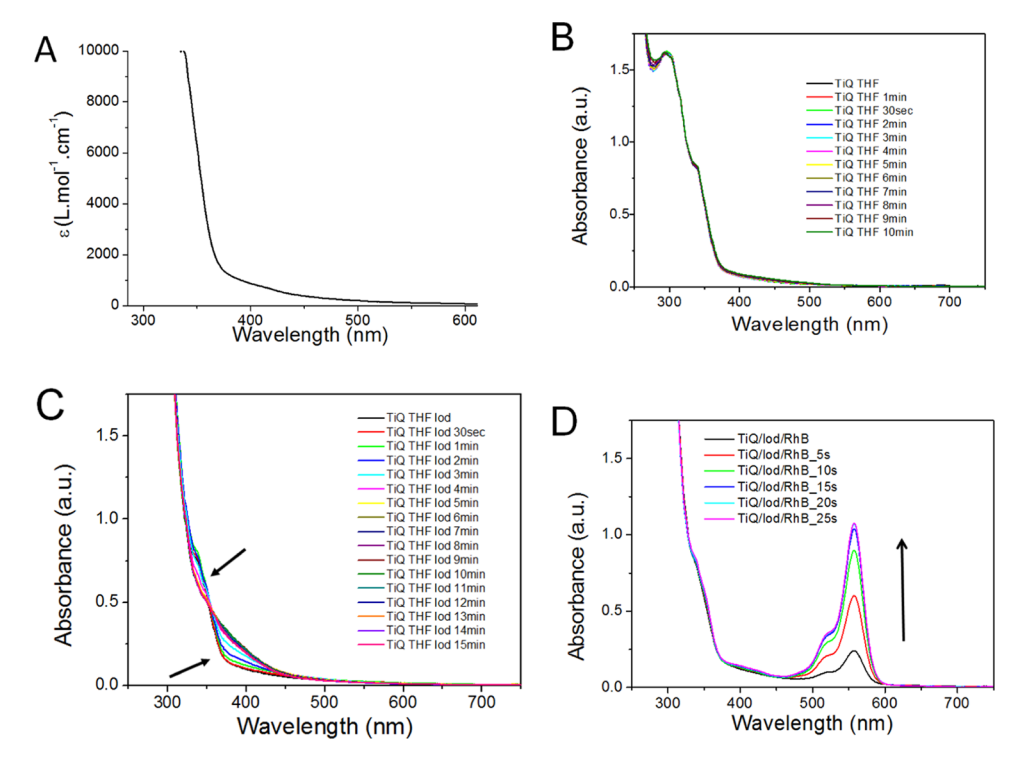


Figure 1. (A) UV-vis absorption spectrum of TiQ in dry THF. Steady-state photolysis of (B) TiQ, (C) TiQ/Iod, and (D) TiQ/Iod/RhB upon LED@385 nm exposure (44 mW/cm²). UV-vis spectra are recorded at different irradiation times under air. [TiQ] = 4.5×10^{-5} M, [Iod] = 10×10^{-3} M, and [RhB] = 5.6×10^{-6} M.

situ during/after exposure. Analogous in situ experiments in toluene were performed at 200 K using temperature control unit ER 4111 VT (X-band; Bruker) with liquid nitrogen as the refrigerant. The total exposure in the EPR cavity was 22 min. The g-values of spin-adducts were determined with an uncertainty of ± 0.0001 using a nuclear magnetic resonance teslameter and integrated frequency counter. The experimental EPR spectra were analyzed by Bruker software WinEPR, and the simulated spectra were calculated using Winsim2002 software 37 or with the EasySpin toolbox. 38

UV–*Vis Absorption Spectra*. UV–vis absorption spectra of the photoinitiating systems were measured under light irradiation using a PerkinElmer Lambda 2 UV–vis spectrophotometer in the 200–1000 nm wavelength range.

Steady-State Photolysis. Steady-state photolysis experiments of TiQ, TiQ/Iod, and TiQ/Iod/RhB were conducted in tetrahydrofuran, under air, and upon LED@385 nm exposure (44 mW/cm²).

Laser Flash Photolysis. The laser flash photolysis setup working at $\lambda_{\rm ex}=385$ nm is based on a nanosecond Nd:TAG laser (Powerlite 9010, Continuum) operating at 5 Hz with 7–8 ns impulsion time. The analyzing system (LP920, Edinburgh Instruments) used a 450-W pulsed xenon arc lamp, a Czerny–Turner monochromator (spectral width = 5 nm, coupled with an emission filter LP314), a fast photomultiplier (PMT R928 fast mode), and a transient digitizer (TDS 340, Tektronix). The sample was contained in a 1 cm cell. Measurements were done at room temperature. The photolysis experiments were carried out in oxygen-free toluene solution of TiQ at room temperature and atmospheric pressure. The molar absorption coefficient of TiQ triplet state and its triplet quantum yield were determined by energy transfer from a standard, i.e., biphenyl, in toluene solution 39 ($\epsilon_{\rm T}$ biphenyl at 360 nm in nonbenzene solution = 37 000 L/(mol cm)).

Photopolymerization Experiments. All of the conditions are given in figure captions. Formulations are deposited on a BaF₂ pellet irradiated under air or under laminated conditions with different LEDs. The thickness of the coatings is 12 μ m for all of the experiments. We can note that all of the formulations containing TiQ (1 wt %) were stirred at room temperature, away from (solar) visible light and none of them have gelled after a night of stirring. The

decrease of the epoxy group contents of EPOX and the acrylate functions of TMPTA are continuously followed by real-time Fourier transform infrared spectroscopy (RT-FTIR, Jasco FTIR 4100) at 790 and 1636 $\rm cm^{-1}$, respectively.

Irradiation Sources. Two light-emitting diodes (LEDs) from Thorlabs were used to initiate the photopolymerization of epoxy and acrylate monomers, i.e., LED@385 nm (12.5 mW/cm²) and LED@405 nm (12.5 and 100 mW/cm²).

Fluorescence Experiments. The absorption measurements were carried out with a PerkinElmer Lambda 2 spectrometer. Steady-state fluorescence spectra were collected from a FluoroMax-4 spectrofluorometer. Emission spectra were spectrally corrected. The interaction rate constants $k_{\rm q}$ between TiQ and Iod were extracted from Stern–Volmer treatment $(I_0/I=1+k_{\rm q}\tau_0[{\rm Iod}])$, where I_0 and I_0 are the fluorescence intensity of TiQ without and with the presence of Iod, respectively, and τ_0 is the lifetime of TiQ without Iod). The fluorescence quantum yields were determined relatively to rhodamine 101 in ethanol ($\Phi_{\rm f}=0.92$) and were corrected for the solvent refractive index.

Cyclic Voltammetry. Cyclic voltammetry measurements of TiQ were carried out at room temperature under N2 atmosphere using an E2 Epsilon auto lab potentiostat/galvanostat under control of a BAS software. A standard three-electrode cell configuration was employed using a glassy carbon working electrode, a platinum wire counter electrode, and a platinum wire as the pseudoreference electrode. ["Bu₄N][PF₆] (0.2 M, THF solution, purified by recrystallization) was used as the supporting electrolyte. All electrochemical data are referenced to the [FeCp₂]⁺/[FeCp₂] redox couple at 0.0 V. The freeenergy change ΔG_{eT} for an electron transfer between TiQ and Iod can be calculated for the classical Rehm-Weller equation ⁴⁰ (eq 5), where $E_{\rm ox}$ (donor), $E_{\rm red}$ (acceptor), $E_{\rm S}$ (or $E_{\rm T}$), $\Delta \bar{E}_{\rm c}$ and F are the oxidation potential of the donor (TiQ), the reduction potential of the acceptor (Iod), the excited (or triplet)-state energy of the sensitizer (TiQ), the Coulombic stabilization energy (negligible for most systems), and Faraday constant, respectively.

$$\Delta G_{\rm et} = F \times (E_{\rm ox}({\rm donor}) - E_{\rm red}({\rm acceptor})) - E_{\rm S}({\rm or} E_{\rm T}) + \Delta E_{\rm c}$$
(5)

Transmission Electron Microscopy (TEM). The thin-film layer of polymer was prepared by cryo-ultramicrotome (thickness less than 100 nm) using a Leica MZ6 stereomicroscope with diamond knife. Both the knife and the specimen are cooled by liquid nitrogen; the room temperature was adjusted at down to -90 °C. The microstructural observations were investigated by bright-field conventional transmission electron microscopy (CTEM) and high-angle annular dark-field scanning transmission electron microscopy (HAADF-STEM) by a transmission electron microscope with a 200 kV FEG TEM (FEI Tecnai F20) with resolution 0.24 nm and equipped with a complete EDS system (windowless Octane SDD detector, 129 eV resolution and 0.5 sr, and TEAM software). The nanoparticle size distribution and average size have been determined by statistical analyses software called CSD. 41

Thermogravimetric Measurements. The thermal degradation of 20 mg of the nanocomposite (TMPTA/EPOX blend and photo-initiated by TiQ/Iod/TT (1/3.7/3% w/w/w)) was studied by TGA analysis. Measurements were carried out on a LabSys Evo TGA-DTA-DSC-1150 °C (SETARAM Instrumentation) under air, with a heating rate of 10 °C/min up to 750 °C.

Mechanical Characterization. The macroscopic mechanical properties of EPOX/TMPTA blend (50/50% w/w) materials based on three different photoinitiating systems, i.e., TiQ/Iod/Trithiol (1/ 3.7/3%, w/w/w), ITX/Iod/Trithiol (1/3.7/3%, w/w/w), and ITX/ Iod/Trithiol/TiO₂ (1/3.7/3/0.5% w/w/w/w), have been tested. The average diameter of TiO2 NPs is 20 nm. Each photosensitive formulation has been introduced in a silicon mold (3.8 cm \times 1.8 cm \times 0.1 cm) and irradiated for 800 s upon LED@405 nm irradiation (100 mW/cm²). The mechanical behavior of the obtained materials was assessed by three-point bending tests. An Instron 5962 universal testing machine equipped with a bending setup and a force cell of 100 N was used. Samples of $40 \times 9 \times 0.7 \text{ mm}^3$ were tested with a crosshead speed of 5 mm/min and a lower support gap of 32 mm (i.e., 80% of the samples length) according to ISO 178 and ASTM D7264 standards. At least three samples per material were tested. The standard deviation of the mechanical values fell within 10% of the average reported quantities.

From such analyses, the force vs displacement plots were obtained. From these results, the flexural stress σ_{θ} the flexural strain ε_{θ} and the flexural modulus $E_{\rm f}$ were calculated according to eqs^{42–44} 2, 3, and 4, respectively

$$\sigma_{\rm f} = 3F\lambda/2wb^2 \tag{6}$$

$$\varepsilon_{\rm f} = 6Db/\lambda^2 \tag{7}$$

$$E_{\rm f} = \lambda^3 m / 4wb^3 \tag{8}$$

where F is the force, λ is the lower support gap, w is the width, b is the thickness, D is the displacement, and m is the slope of the force vs displacement plot taken between 0.25 and 0.5% of the flexural strain $\varepsilon_{\rm f}$ according to ISO 178 and ASTM D7264 standards.

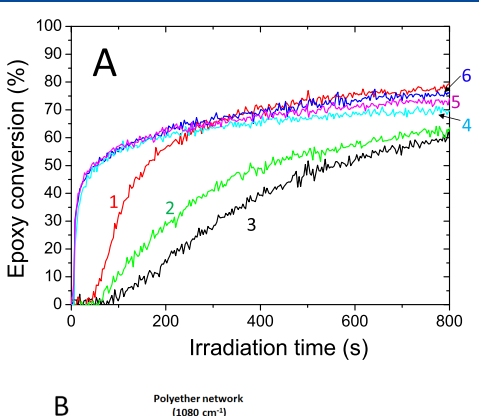
RESULTS AND DISCUSSION

Behavior under Light Irradiation. The absorption spectrum of the investigated compound, TiQ, in dry tetrahydrofuran (THF) is displayed in Figure 1A. The absorbance maxima of TiQ at 385 nm (ε = 1100 M⁻¹ cm⁻¹) and 405 nm (811 M⁻¹ cm⁻¹) ensure an interesting overlap with the emission spectra of the LED bulb at 385 and 405 nm. The value of molar absorption coefficient of TiQ is similar to quinoline derivative compounds described by Merlo et al. ⁴⁵ The absorption of TiQ red-shifts with the complexation of the titanium ion in comparison to free quinoline. The steady-state photolysis images of TiQ, TiQ/Iod, and TiQ/Iod/RhB upon 385 nm LED exposure in dry THF and under air are given in Figure 1B–D, respectively. Under light irradiation, TiQ alone is not photobleached (Figure 1B); on the contrary, a fast

photobleaching of the TiQ/Iod photosystem can be readily observed.

The ability to generate protons using TiQ as a photosensitizer of Iod is demonstrated in Figure 1D. In this experiment, both compounds are mixed together in the presence of rhodamine B (RhB) as acid indicator. 46,47 Interestingly, a gradual increase of the lowest-energy band of the acid form of RhB at 550 nm is observed upon LED@385 nm exposure with TiQ/Iod. This experiment demonstrates the ability of TiQ/Iod to generate photoacids, which may initiate the cationic photopolymerization of epoxy monomers. According to investigations by Pappas et al., 48-50 the photolysis of Iod leads to the formation of a radical cation intermediate ([MePhI-PhMeI]+•), which is oxidized by Iod to yield [MePhI+-PhMeI], together with a diphenyliodine radical ((MePh)₂I•) and photoacids. It should be noted that, in the same conditions of irradiation (LED@385 nm), Iod alone does not generate any Brønsted acid (H⁺).

Ring-Opening Polymerization of Epoxides. The photopolymerization of EPOX under air in the presence of the TiQ/ Iod photoinitiating system was carried out using 385 and 405 nm LED irradiation, compared to the ITX/Iod model system. The kinetic profiles and the conversions are summarized in Figure 2 and Table 1, respectively. When Iod is used alone, no photopolymerization is observed under UVA or visible light as Iod absorbs and works below 300 nm. When using TiQ/Iod, the cationic polymerization of EPOX successfully proceeds (Figure 2A), thus demonstrating the photosensitizer behavior of TiQ under two different wavelengths (385 and 405 nm). In



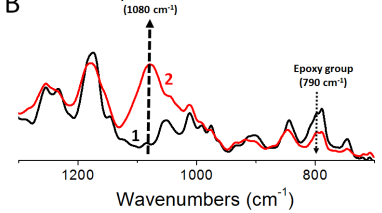


Figure 2. (A) Cationic photopolymerization of EPOX under air in the presence of (1) TiQ/Iod (1/3.7%, w/w) upon LED@385 nm irradiation (44 mW/cm²), (2) TiQ/Iod (1/3.7%, w/w) upon LED@405 nm irradiation (100 mW/cm²), (3) TiQ/Iod (1/3.7%, w/w) upon LED@385 nm irradiation (12.5 mW/cm²), (4) ITX/Iod (1/3.7%, w/w) upon LED@385 nm irradiation (12.5 mW/cm²), (5) ITX/Iod (1/3.7%, w/w) upon LED@385 nm irradiation (44 mW/cm²), and (6) ITX/Iod (1/3.7%, w/w) upon LED@405 nm irradiation (100 mW/cm²). (B) FTIR spectra of the TiQ/Iod/EPOX formulation (1) before light exposure and (2) after 800 s irradiation upon LED@385 nm irradiation (12.5 mW/cm²). Thickness = 12 μm.

Table 1. EPOX Conversions Obtained under Air upon LED@385 nm and LED@405 nm for 800 s Exposure to Different Light Intensities in the Presence of TiQ/Iod (1/3.7%, w/w) or ITX/Iod (1/3.7%, w/w)^a

	EPOX conversion (%)					
	LED@385 nm intensity (mW/cm²)		LED@-	LED@405 nm intensity (mW/cm²)		
photoinitiating systems	12.5	44	12.5	44	100	
TiQ/Iod	60	80	np	np	60	
ITX/Iod	69	72			75	

^anp = no polymerization.

addition, a new peak ascribed to the formation of a polyether network appears at 1080 cm⁻¹, therefore confirming the cationic polymerization of EPOX (Figure 2B). TiQ is particularly well adapted with LED@385 nm. Accordingly, the final conversion reaches 80% after 800 s exposure (44 mW/cm²), whereas such system (EPOX/TiQ/Iod) does not polymerize at the same intensity with LED@405 nm. This could mainly be explained by the lower molar absorption coefficient at 405 nm ($\varepsilon_{405 \text{ nm}} = 811 \text{ M}^{-1} \text{ cm}^{-1}$) than that observed at 385 nm ($\varepsilon_{385 \text{ nm}} = 1100 \text{ M}^{-1} \text{ cm}^{-1}$). A higher intensity at 405 nm (100 mW/cm²) is needed to initiate the EPOX photopolymerization. It is also interesting to note that a period of inhibition for all of the cationic photopolymerization profiles is observed, thus likely implying a reaction pathway involving the triplet state of TiQ (see section 3, Mechanistic Studies). For comparison, ITX/Iod was tested (ITX, i.e., 2isopropylthioxanthone, ¹⁸ is a well-known photosensitizer). ITX is well adapted for the LEDs at 385 or 405 nm irradiation, as its absorption maxima is in the range of 380-420 nm, and the sensitized decomposition of Iod in the presence of ITX has been shown to occur through an electron-transfer reaction to produce Brønsted acids, which lead to the cationic photopolymerization of EPOX. 18 The final conversion after 800 s of irradiation remains approximately the same as the TiQ/Iod system at 385 nm, but remains slightly higher at 405 nm. A comparable reaction pathway for TiQ/Iod is displayed in

Free-Radical Polymerization of Acrylates. The freeradical polymerizations of TMPTA under air/laminate conditions, and in the presence of TiQ/Iod/Trithiol, ITX/ Trithiol, or ITX/MDEA photoinitiating systems using LED@ 405 nm are displayed in Figure 3. The final conversions of all of the photosensitive systems used are summarized in Table 2. The film thickness has been set at 12 μ m to maximize oxygen contact. Two photoinitiating systems have been used as references, i.e., ITX/Trithiol and ITX/MDEA, and compared to the TiQ-based systems. Figures S1-S3 display all of the kinetics profiles for the free-radical polymerization of TMPTA with ITX/Trithiol, ITX/MDEA, and TiQ/Iod/Trithiol photoinitiatings systems, respectively, upon LEDs@385 and 405 nm irradiation. Thioxanthone derivatives^{51–53} in conjunction with some H-donors are highly efficient photoinitiating systems for free-radical photopolymerization of acrylate monomers. Tertiary amines such as MDEA play a dual role in the photopolymerization reaction. Besides hydrogen donation, MDEA reacts with O₂, thereby reducing the inhibition of free-radical polymerization by oxygen. The second common method used for oxygen depletion consists of the addition of thiol compounds. $^{55-58}$

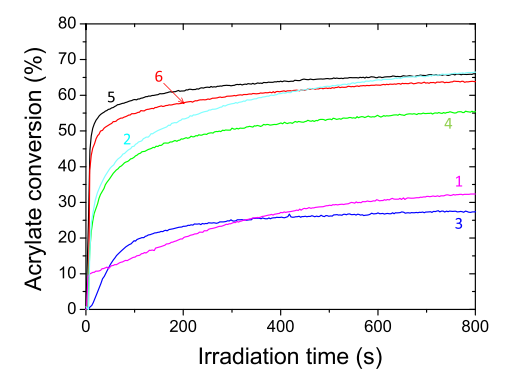


Figure 3. Free-radical photopolymerization of TMPTA upon LED@ 405 nm irradiation (100 mW/cm²) with (1) TiQ/Iod/Trithiol (1/ 3.7/3%, w/w/w) under air, (2) TiQ/Iod/Trithiol (1/3.7/3%, w/w/w) in laminate, (3) ITX/Trithiol (1/3%, w/w) under air, (4) ITX/Trithiol (1/3%, w/w) in laminate, (5) ITX/MDEA (1/3%, w/w) under air, and (6) ITX/MDEA (1/3%, w/w) in laminate. Thickness = 12 μ m.

Table 2. TMPTA Conversions Obtained under Air and in Laminate Conditions upon LED@385 nm and LED@405 nm for 800 s Exposure to Different Light Intensities in the Presence of TiQ/Iod/Trithiol (1/3.7/3%, w/w/w), TiQ/Iod (1/3.7%, w/w), Iod/Trithiol (3.7/3%, w/w), ITX/Trithiol (1/3%, w/w/w), and ITX/MDEA (1/3% w/w)

	TMPTA conversion (%)						
	LED@385 nm intensity (mW/cm²)		405 nm mW/cm ²)				
photoinitiating system	12.5	12.5	100				
TiQ/Iod/Trithiol	21 ^a , 60 ^b	35 ^a , 70 ^b					
TiQ/Iod	np ^a , 30 ^b	np ^a , 45 ^b	np ^a , 50 ^b				
Iod/Trithiol	np ^a , 19 ^b	np ^{a,b}					
ITX/Trithiol	31 ^a , 52 ^b	23 ^a , 48 ^b	27 ^a , 53 ^b				
ITX/MDEA	45 ^a , 62 ^b	55 ^a , 60 ^b	63 ^a , 67 ^b				

^aUnder air. ^bIn laminate, np = no polymerization.

After being exited under light irradiation and in the presence of hydrogen donors¹⁸ such as MDEA or Trithiol, the photolysis of aromatic ketones leads to the formation of both radicals derived from the carbonyl compound (ketyl-type radical) and other radicals derived from the hydrogen donor via an H-abstraction mechanism. The generated α -aminoalkyl or thiyl radicals⁵⁸ can therefore initiate the photopolymerization even in air. Indeed, these radicals react with oxygen to form peroxyl radicals, which are able to abstract hydrogen atom from MDEA or thiol group; thus, α -aminoalkyl or thiyl radicals are regenerated. This fact is further corroborated since the photopolymerization of TMPTA with both ITX/MDEA and ITX/Trithiol photoinitiating systems is evaluated at around 30% even in air (Table 2). However, the ITX/ MDEA photoinitiating system appears more reactive than the ITX/Trithiol one: indeed, the reactivity of the α -aminoalkyl radicals is higher than that observed for thiyl radicals toward the acrylate monomer. 59-61

Under the same conditions, and in the absence of Iod, no polymerization was observed in air or in laminate conditions with TiQ since it is not able to abstract H as a ketone PI did. When TiQ is combined with Iod, the photopolymerization of TMPTA occurs only under laminate conditions. This suggests the formation of phenyl-derived radicals by an electron-transfer

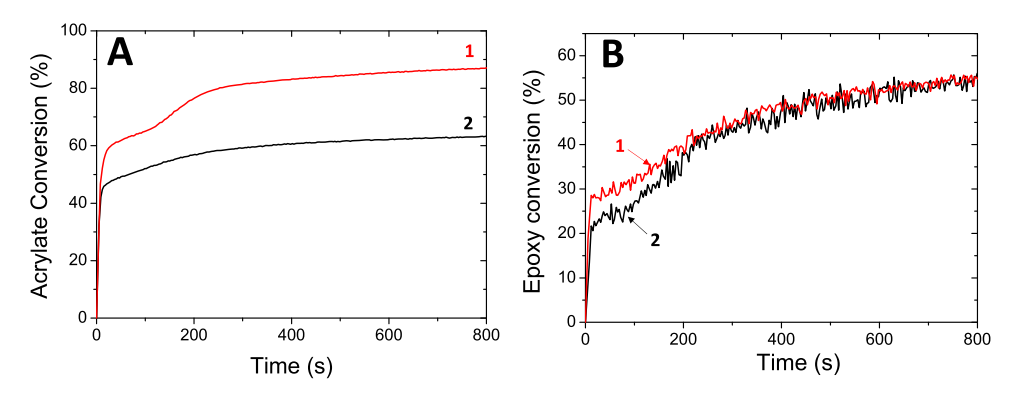


Figure 4. Photopolymerization profiles of an EPOX/TMPTA blend (50/50%, w/w) in the presence of TiQ/Iod/Trithiol (1/3.7/3%, w/w/w) upon LED@405 nm (100 mW/cm²) in laminate (A and B: curves 1) and under air (A and B: curves 2). Thickness = 12 μ m.

reaction between TiQ and Iod (see section 3, Mechanistic Studies); according to the literature, such radicals can afford to initiate the free-radical polymerization. However, under air, phenyl-derived radicals are scavenged by oxygen (peroxyl radicals) and are unable to initiate the photopolymerization of TMPTA. With the multicomponent photoinitiating systems containing TiQ/Iod/Trithiol, the photopolymerization of TMPTA successfully takes place even in the presence of air; nevertheless, the final conversion remains higher in laminate conditions than under air without any period of inhibition. This could be explained by the presence of thiol functionalities, which are well adapted to overcome oxygen scavenging in radical polymerization.⁸ Indeed, a direct hydrogen-transfer reaction may occur under air between the peroxyl radicals and trithiol; thiyl radicals are thus generated and lead to the consumption of acrylate function. It is also interesting to show that the use of Iod/trithiol alone fails to initiate the photopolymerization of TMPTA under air and the final conversion remains much lower than TiQ/Iod/Trithiol in laminate.

Synthesis of Interpenetrating Networks. Interpenetrated polymer networks (IPN) can also be obtained through a concomitant cationic/radical photopolymerization of a TMPTA/EPOX blend (50/50% w/w) using a TiQ/Iod/ Trithiol combination under air or in laminate upon visible light irradiation (LED@405 nm, 100 mW/cm²) (Figure 4). Some investigations in the literature 60,62-64 have proposed such a mixture (TMPTA/EPOX blend) for demonstrating the dual role of the photoinitiating systems for the concomitant cationic/radical photopolymerization. As described elsewhere for other systems,8 the final conversions of TMPTA are higher in laminate (87%, Figure 4A-1) than under air (63%, Figure 4A-2). However, the final conversions are not influenced by air/laminate conditions when considering EPOX polymerization (Figure 4B); the oxygen scavenging effect plays an important role in the free-radical polymerization of TMPTA rather than in the cationic photopolymerization of EPOX, as the radicals are predominantly consumed by oxygen to form peroxy radicals, which are unable to initiate the polymerization. Interestingly, the final conversion of TMPTA under air (in the EPOX/TMPTA blend) with TiQ/Iod/Trithiol photoinitiating system is twice higher than that observed with TMPTA alone (Figure 3, Table 2). As previously described in the literature, 1,65 EPOX has a labile H that phenyl-derived radicals are able to abstract, thus leading to the formation of carbonderived radicals on the EPOX backbone (epoxy(-H)*). The latter radical can indeed add on the acrylate double bond of TMPTA and increase the acrylate conversion over time. A similar mechanism has been demonstrated with camphorquinone. The formation of carbon-centered radicals may thereafter be oxidized by Iod to form cationic species, ^{1,65} i.e., epoxy_(-H)⁺ and radical cation MePhI⁺. These results could explain the increase of the initial rate constant of EPOX (Figure 4B) in comparison to that observed in Figure 2A in the first second of the photopolymerization process (Table 3).

Table 3. EPOX/TMPTA Blend (50/50%, w/w) Conversions Obtained under Air and in Laminate upon LED@405 nm (100 mW/cm²) for 800 s Exposure in the Presence of TiQ/Iod/Trithiol (1/3.7/3%, w/w/w)

	LED@405 nm (100 mW/cm ²)			
	air (%)	laminate (%)		
acrylate conversion	63	87		
epoxy conversion	55	55		

Mechanistic Studies. The maximum absorption and emission wavelengths and other photophysical properties of TiQ are summarized in Table 4. The proposed mechanism (rrr1-rrr9) reflects the polymerization process under argon. Reactions in air as well as the proposed mechanism of the in situ synthesis of Ti-based NPs are described in Section 3.7 to avoid confusion.

Proposed Mechanism under Argon. According to the studies of other related photoinitiating systems using Iod, the proposed sequence holds true as confirmed by the fluorescence, nanosecond laser flash photolysis, and EPR experiments reported below.

$$TiQ(h\nu) \rightarrow {}^{1}TiQ \rightarrow {}^{3}TiQ$$
 (r1)

 1,3 TiQ + (MePh)₂I⁺(Iod)

$$\rightarrow \text{TiQ}^{\bullet+} + (\text{MePh})_2 \text{I}^{\bullet}$$

$$\rightarrow \text{TiQ}^{\bullet +} + \text{MePh}^{\bullet} + \text{MePhI}$$
 (r2)

$$MePhI + TiQ^{\bullet +} \rightarrow MePhI^{+ \bullet} + TiQ$$
 (r3)

$$MePhI^{+\bullet} + MePhI \rightarrow [MePhI - PhMeI]^{+\bullet}$$
 (r4)

 $[MePhI - PhMeI]^{+\bullet} + (MePh)_2I^+$

$$\rightarrow [MePhI^{+} - PhMeI] + \mathbf{H}^{+} + (MePh)_{2}I^{\bullet}$$
 (r5)

$$(MePh)_2I^{\bullet} \rightarrow MePhI + MePh^{\bullet}$$
 (r6)

Table 4. Photophysical Properties of TiQ^b

λ_{\max}^{Em} (nm)	$E_{\rm S}^{a}$	$\Delta G_{\rm eT}(S)^a$	$arphi_{ ext{Fluo}}^{}a}$	λ_{\max}^{Ta} (nm)	$E_{\rm T}^{a}$ (eV)	$\varepsilon_{\mathrm{T}}^{a} \; (\mathrm{M}^{-1} \; \mathrm{cm}^{-1})$	$\Delta G_{\rm et}({ m T})^a~({ m eV})$	${\phi_{ m T}}^a$
420	3.36	-2.80	0.053	440	2.82	18390	-2.26	0.87
^a In THF. ^b Tolu	ene.							

$$MePh^{\bullet} + RS - H(Trithiol) \rightarrow MePh - H + RS^{\bullet}$$
 (r7)

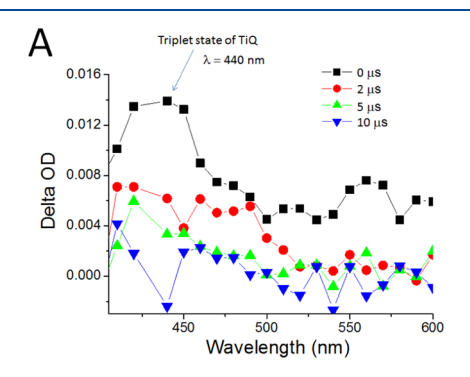
$$RS^{\bullet} + R' - CH = CH_2(TMPTA)$$

 $\rightarrow R' - CH^{\bullet} - CH_2 - SR$ (r8)

$$R' - CH^{\bullet} - CH_2 - SR + RS - H$$

 $\rightarrow R' - CH_2 - CH_2 - SR + RS^{\bullet}$ (r9)

Transition absorption spectra of **TiQ** are displayed in Figure 5A, and reveal the triplet state ³TiQ (rrr1) at around 440 nm



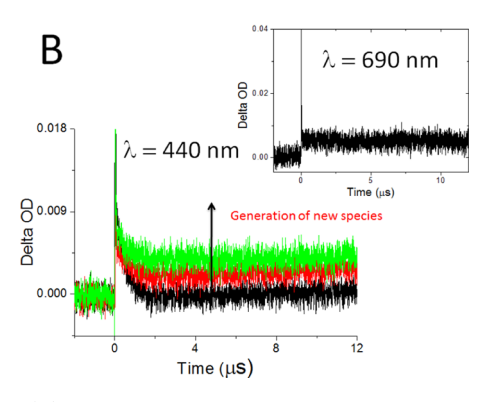


Figure 5. (A) Transition absorption spectra of the **TiQ** complex under argon atmosphere after 0, 2, 5, and 10 μ s ($\lambda_{\rm ex} = 385$ nm). (B) Decay of the **TiQ** triplet state at 440 nm with the addition of Iod. Inset: Transient signal ($\lambda_{\rm abs} = 690$ nm) of a iodonium derivative compound after the irradiation ($\lambda_{\rm ex} = 385$ nm) of **TiQ**/Iod photosensitive system under argon atmosphere. Solvent = toluene.

as described for other quinoline derivative compounds.⁴⁵ The quenching rate constants of ^3TiQ by oxygen and Iod were evaluated at $k_{\rm q}({\rm O}_2) > 10^9~{\rm M}^{-1}~{\rm s}^{-1}$ (Figure S4) and $k_{\rm q}({\rm Iod}) > 10^8~{\rm M}^{-1}~{\rm s}^{-1}$ (Figure SB), respectively. According to Figure SB, the addition of Iod to excited TiQ leads to the formation of a new species absorbing in the visible range (690 nm), which could be attributed to 4-methylphenyliodinium radical cation (MePhI+•) (rrr3). Intermediate MePhI+• is postulated to react with MePhI to produce a new transient species 48,49 [MePhI-PhMeI]+• (rrr4). This intermediate may be oxidized by diphenyliodonium ion to yield [MePhI+PhMeI], together with a diphenyliodine radical ((MePh)₂I•) and photoacids 48,49 (H+) in rrr5. (MePh)₂I• is known to be unstable 48,49 and

decomposes to iodobenzene and phenyl(4-methyl) radical (MePh $^{\bullet}$) in rrr6 (EPR experiments; Figure 7). For a photoinduced electron transfer reaction to be thermodynamically feasible, $\Delta G_{\rm eT}$ has to be negative. Therefore, the $\Delta G_{\rm eT}$ values are useful to the most valuable photochemistry pathways. In our conditions, the calculation of the free-energy change ($\Delta G_{\rm eT}({\rm T})$) calculated from the Rehm–Weller equation (eq 5, cyclic voltametry in Experimental Section) for the $^3{\rm TiQ/Iod}$ electron-transfer reaction demonstrates a fast and spontaneous process: $\Delta G_{\rm eT} = -2.26$ eV ($E_{\rm ox}$ of TiQ = +0.46 V/SCE or -0.1 V/[FeCp₂]+/[FeCp₂] redox couple, as measured by cyclic voltammetry in this work in THF (see Supporting Information Figure S5); $E_{\rm Red}$ of Iod = -0.2 V/SCE, 8,36,37 triplet state energy $E_{\rm T}$ of TiQ = 2.82 eV as extracted from the transition absorption spectrum).

Fluorescence quenching experiment of TiQ by Iod in THF is displayed in Figure 6; this allows determining whether the

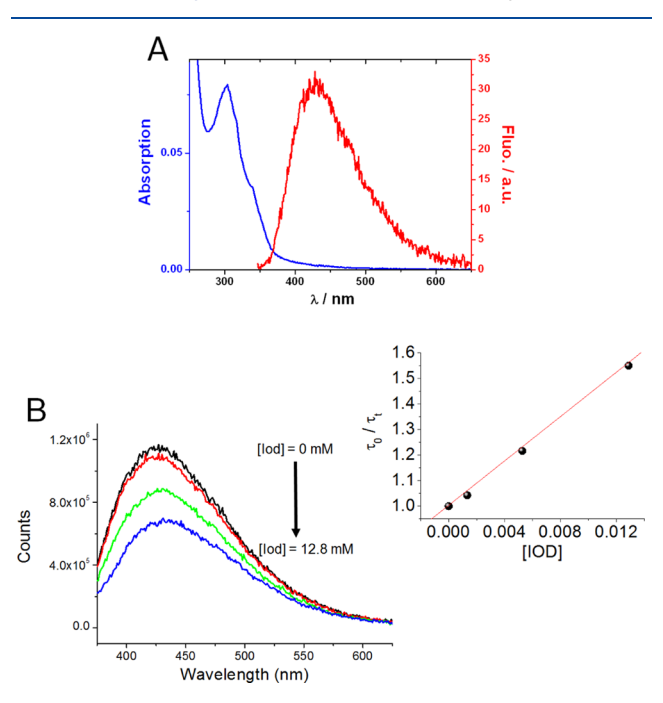


Figure 6. (A) Absorbance and emission spectra of TiQ in THF: the blue curve corresponds to the ground-state absorption spectrum of TiQ, and the red curve corresponds to the emission spectrum of TiQ ($i_{\rm ex}=370$ nm). (B) Fluorescence quenching of TiQ by Iod in THF ($\lambda_{\rm ex}=370$ nm). Inset: evolution of the fluorescence intensity as a function of [Iod].

singlet state of TiQ is involved in the photoinitiating process or not. The free-energy change ($\Delta G_{\rm eT}(S)$) for the $^1{\rm TiQ/Iod}$ electron-transfer reaction was evaluated at -2.8 eV, and the associated dynamic Stern–Volmer constants (KSV) between TiQ and Iod are evaluated at 132 M $^{-1}$. The electron-transfer quantum yield $\Phi_{\rm eT}$ of TiQ/Iod in our case and calculated according to eq 9 is high at 0.79 (for [Iod] = 9.27 \times 10 $^{-2}$ M)

$$\Phi_{\text{et}} = k_{\text{q}} \tau_0 [\text{Iod}] / (1 + k_{\text{q}} \tau_0 [\text{Iod}])$$
(9)

However, according to the low fluorescence quantum yield of TiQ (0.053), its high triplet quantum yield³⁹ (0.87), and the inhibition period observed in the EPOX photopolymerization (Figure 2), we can properly expect that the photoinduced process in the TiQ/Iod system mainly occurs from the triplet state, whereas the singlet state is certainly involved in a minor component of the polymerization process.

In line with rrr2 and rrr6, the photoexcitation of TiQ/Iod/benzene in the presence of DMPO spin trap under argon using LED@400 nm source resulted in the immediate generation of EPR signals shown in Figure 7. To achieve the best fit of the

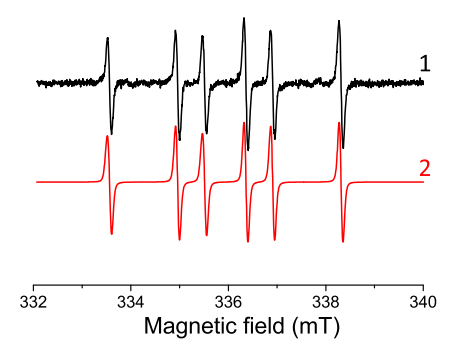


Figure 7. Experimental (1) and simulated (2) EPR spectra monitored in benzene solution of TiQ/Iod under argon upon 450 s in situ LED@400 nm exposure and under air upon 450 s in situ LED@400 nm exposure. EPR spectrometer settings: microwave frequency, ~9.432 GHz; microwave power, 10.94 mW; center field, 335.94 mT; sweep width, 7 mT; gain, 2.52 × 10⁵; modulation amplitude, 0.05 mT; sweep time, 45 s; time constant, 10.24 ms; number of scans, 10.

experimental six-line spectrum characterized by the asymmetric signal intensities, abundance of two DMPO spin-adducts of carbon-centered radicals (Figure 7) with slightly different spin-Hamiltonian parameters was included in the simulation. The dominant signal with relative concentration (c_{rel}) of 70% characterized with $a_{\rm N}$ = 1.399 mT, $a_{\rm H}{}^{\beta}$ = 1.956 mT, and g = 2.0060 was assigned to *DMPO-(4-methylphenyl)⁶⁷ spinadduct derived from the ³TiQ/Iod electron-transfer reaction and the hemolysis of the carbon-iodine bond of Iod. The spin-Hamiltonian parameters of the second signal ($a_N = 1.415$ mT, $a_H^{\beta} = 1.957$ mT, g = 2.0061) are compatible with the DMPO adduct of an aromatic carbon-centered radical, produced most probably from quinoline ligand (TiQ*+, rrr2). This EPR result clearly highlights that MePh is reactive toward acrylate double bonds²⁹ and leads, in laminated conditions, to the free-radical photopolymerization of TMPTA with TiQ/Iod photoinitiating system (Table 2, Figure S3). The photorelease of acids (H+) in rrr5 is demonstrated in Figure 1D and is confirmed by the cationic photopolymerization of EPOX shown in Figure 2. Finally, the acrylate consumption of TMPTA (Figure 3), with the TiQ/ Iod/Trithiol photoinitiating system under light irradiation, is consistent with the proposed reactions shown in rrr7-rrr9. Indeed, the in situ irradiation of TiQ/Iod/Trithiol solutions containing the DMPO spin trap using LED@400 nm source revealed an EPR spectrum (Figure 8) with dominating signals characterized by the spin-Hamiltonian parameters $a_N = 1.351$ mT, $a_{\rm H}{}^{\beta}$ = 1.181 mT, $a_{\rm H}{}^{\gamma}$ = 0.093 mT, $a_{\rm H}{}^{\gamma}$ = 0.072 mT, and g = 2.0059 (relative concentration, 98.8%) correlating well with the ${}^{\bullet}$ DMPO-SR spin-adduct. Furthermore, a low-intensity six-line signal ($a_N = 1.429 \text{ mT}$, $a_H^{\beta} = 1.929 \text{ mT}$, g = 2.0057(rel. conc., 1.2%) observed in the EPR spectrum (Figure 8)

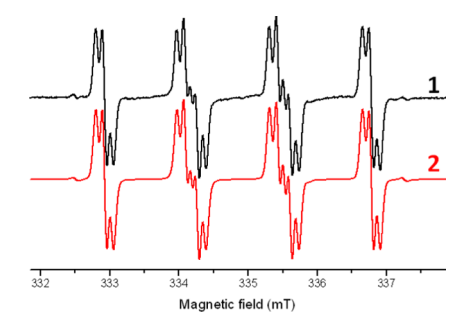


Figure 8. Experimental (1, black trace) and simulated (2, red trace) EPR spectra of DMPO spin-adducts obtained upon in situ LED@400 nm exposure of TiQ/Iod/Trithiol/DMPO in benzene under argon. EPR spectrometer settings: microwave frequency, ~9.448 GHz; microwave power, 10.03 mW; center field, 335.2 mT; sweep width, 6 mT; gain, 2.00 c 10⁵; modulation amplitude, 0.025 mT; scan, 84 s; time constant, 20.48 ms; number of scans, 10.

can be assigned to the *DMPO-(4-methylphenyl) spin-adduct. The detected DMPO spin-adducts confirmed the formation of thiyl radicals, along with the generation/consumption of MePh* species (rrr7), which further corroborates our proposed reaction mechanism, and is in accordance with the literature. In light of these results, MePh* and RS* react with TMPTA acrylate double bonds, leading to a high final acrylate conversion in laminate with the TiQ/Iod/Trithiol photo-initiating system (Table 2, Figure 3, and Figure S3).

Proposed Mechanism in Air and Understanding the Synthesis of Ti-Based NPs. Under air conditions and due to the increased solubility of molecular oxygen in benzene, the EPR spectra monitored in the irradiated solutions TiQ/Iod/DMPO/benzene are characterized with substantially broadened spectral lines (Figure 9). The simulated spectrum was

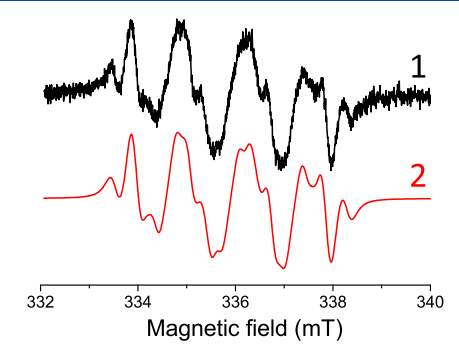
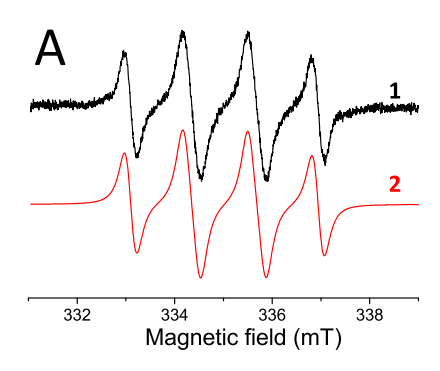


Figure 9. Experimental (1) and simulated (2) EPR spectra monitored in benzene solution of TiQ/Iod/DMPO under air upon 450 s in situ LED@400 nm exposure. EPR spectrometer settings: microwave frequency, \sim 9.432 GHz; microwave power, 10.94 mW; center field, 335.94 mT; sweep width, 7 mT; gain, 2.52 \times 10⁵; modulation amplitude, 0.05 mT; sweep time, 45 s; time constant, 10.24 ms; number of scans. 10.

fitted considering the presence of two dominated DMPO carbon-centered spin-adducts, i.e., *DMPO-OR1 ($a_{\rm N}=1.307$ mT, $a_{\rm H}{}^{\beta}=0.664$ mT, $a_{\rm H}{}^{\gamma}=0.178$ mT, g=2.0061) and *DMPO-OR2 ($a_{\rm N}=1.374$ mT, $a_{\rm H}{}^{\beta}=1.157$ mT, $a_{\rm H}{}^{\gamma}=0.079$ mT, g=2.0060). The detected radicals reflect the proposed generation of carbon-centered radicals (MePh* and TiQ**) upon exposure of TiQ/Iod and their subsequent reaction with molecular oxygen to produce ROO* radicals, which are detected as the corresponding *DMPO-OR spin-adduct



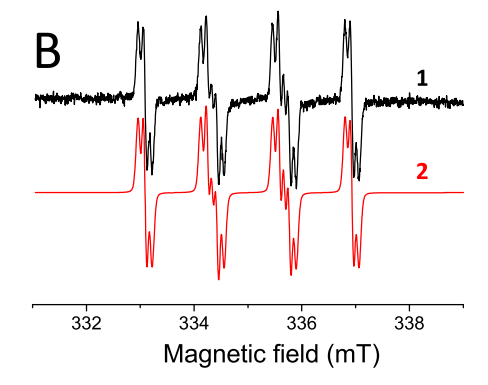


Figure 10. Experimental (1) and simulated (2) EPR spectra monitored in benzene solution of TiQ/Iod/Trithiol/DMPO: (A) under air upon 450 s in situ LED@400 nm exposure and (B) solution from experiment (A) measured in the dark after a short postradiation saturation with argon. EPR spectrometer settings: microwave frequency, ~9.448 GHz; microwave power, 10.03 mW; center field, 335.0 mT; sweep width, 6 mT; gain, 2.00 or 2.52×10^5 ; modulation amplitude, 0.025 mT; sweep time, 84 or 45 s; time constant, 20.48 ms or 10.24; number of scans, 10.

(oxygen-centered radicals) from the decomposition of peroxyl radical adducts.⁶⁸ These results are in accordance with the absence of polymerization of the TMPTA/TiQ/Iod system under air (Table 2, Figure S3). Indeed, peroxyl radicals are inactive toward the acrylate double bonds.

However, the addition of Trithiol reveals additional new EPR signals (Figure 10), which are attributed to the thiyl (RS*) and peroxyl radicals. Peroxyl radicals formed by the oxygen scavenging of carbon- and sulfur-centered radicals (rrr10) are also capable of abstracting hydrogen atoms from thiol and regenerate thiyl radicals (rrr11). This explains why a polymerization occurs with TiQ/Iod/Trithiol under air (Table 2, Figure 3, and Figure S3).

$$P \cdot + O_2 \rightarrow POO \cdot$$
 (r10)

$$POO \cdot + RSH \rightarrow POOH + RS \cdot$$
 (r11)

When the TiQ/Iod/benzene solutions were continuously irradiated (LED@400 nm) in air without the use of DMPO (Figure 11), the EPR spectrum of superimposed paramagnetic signals was obtained. Despite the limited resolution of the hyperfine structure due to the significant line broadening caused by the molecular oxygen dissolved in benzene, ⁶⁹ the EPR spectral characteristics (spin-Hamiltonian parameters $a_{\rm N}$ = 0.9310 mT, $a_{\rm H}$ = 0.365 mT, $a_{\rm H}$ = 0.276 mT, g = 2.0058) are well compatible with previously published data for substituted

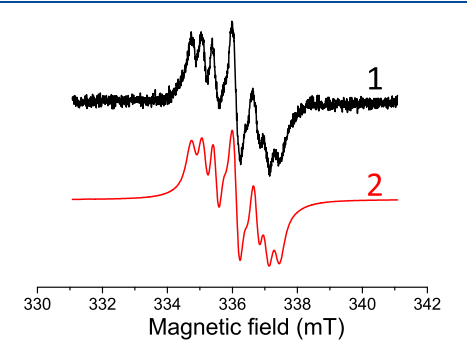


Figure 11. Experimental (1) and simulated (2) EPR spectra monitored in benzene solution of TiQ/Iod under air (without DMPO) upon 900 s in situ LED@400 nm exposure. EPR spectrometer settings: microwave frequency, \sim 9.435 GHz; microwave power, 11.21 mW; center field, 336.12 mT; sweep width, 7 mT; gain, 2.52 \times 10⁵; modulation amplitude, 0.1 mT; sweep time, 90 s; time constant, 20.48 ms; number of scans, 10.

quinoline N-oxyl radicals. 70,71 In addition to the EPR signal, the simulation analysis of the EPR spectrum measured upon photoexcitation (Figure 11) also evidenced the presence of a triplet signal without a resolvable hyperfine coupling. The latter ($a_N = 0.634 \text{ mT}$, g = 2.0056) is also assigned to a *N*-oxyl radical possessing delocalized π -electrons over the π -conjugated systems.⁷² These later results undoubtedly reflect the photoinduced oxidative cleavage of metal-ligand bond upon the photoactivation of TiQ in the presence of molecular oxygen or singlet oxygen. Indeed, the photoinduced formation of singlet oxygen is frequently monitored by EPR spectroscopy, detecting the generation of nitroxide radicals, Tempone, produced by the oxidation of 4-oxo-2,2,6,6-tetramethylpiperidine 73,74 (TMPO). Interestingly, the stable nitroxide radical Tempone, which has a signature EPR spectrum⁷⁵ formed via the oxidation of TMPO, appears when TiQ/Iod/TMPO/ benzene/air solution is irradiated upon LED@400 nm (Figure 12). Therefore, the EPR spectrum observed reveals a low-

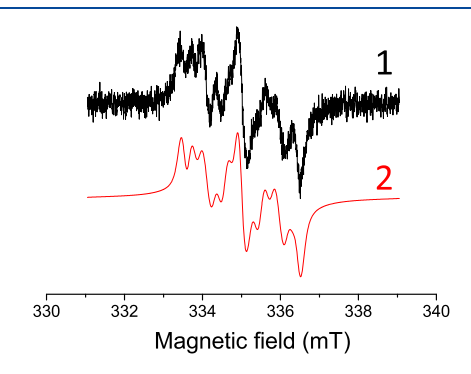


Figure 12. Experimental (1) and simulated (2) EPR spectra monitored in benzene solution of TiQ/Iod/TMPO under air after 450 s irradiation (LED@400 nm). EPR spectrometer settings: microwave frequency, ~9.443 GHz; microwave power, 10.03 mW; center field, 335.05 mT; sweep width, 7 mT; gain, 2.52×10^5 ; modulation amplitude, 0.1 mT; sweep time, 45 s; time constant, 20.48 ms; number of scans, 10.

intensity three-line signal of Tempone ($a_{\rm N}$ = 1.468 mT, g = 2.0055), superimposed on the signals of quinoline N-oxyl radicals ($a_{\rm N}$ = 0.9310 mT, $a_{\rm H}$ = 0.365 mT, $a_{\rm H}$ = 0.276 mT, g = 2.0058).

In conclusion, when the photoinitiating system TiQ/Iod is irradiated in air, singlet oxygen 1O_2 is generated along with peroxyl radicals. 1O_2 leads to the photoinduced oxidative

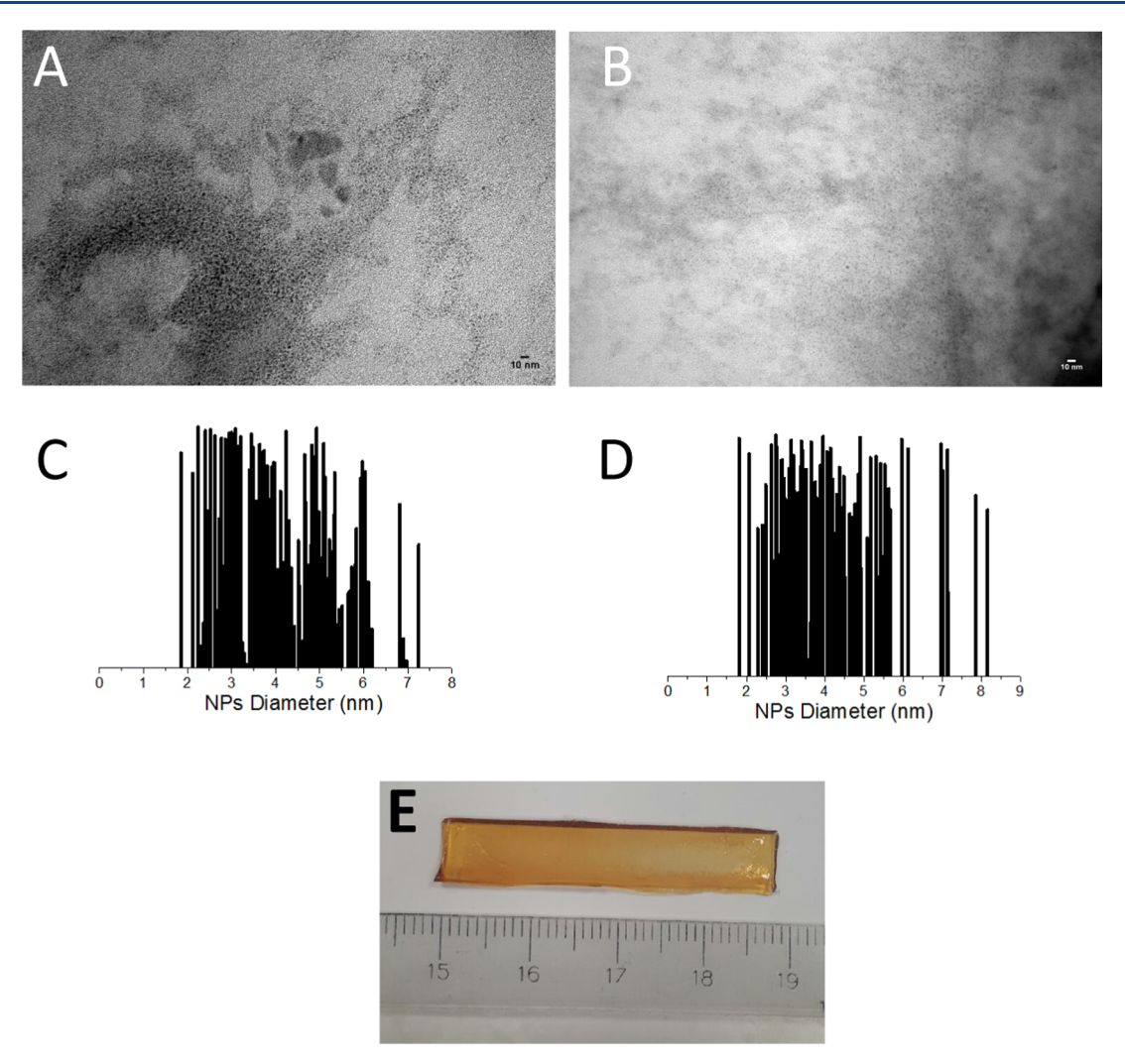


Figure 13. TEM images of Ti-based NPs inside coatings from (A) TiQ/Iod/EPOX system upon an LED@385 nm exposure (44 mW/cm²) under air and (B) EPOX/TMPTA blend (50/50%, w/w) in the presence of TiQ/Iod/Trithiol upon a LED@405 nm exposure (100 mW/cm²) under air. Irradiation time = 800 s. (C, D) NPs diameter inside the coatings from TiQ/Iod/EPOX and EPOX/TMPTA/TiQ/Iod/Trithiol photoinitiating systems, respectively. (E) Optical image of the photosynthesized materials with the TiQ/Iod/Trithiol/TMPTA/EPOX system after 800 s of irradiation under air upon LED@405 nm exposure (100 mW/cm²).

cleavage of the metal (Ti)—ligand bond (quinoline ligand), resulting in the formation of oxygen-centered radicals (*N*-oxyl radicals, RNO*) and probably metal oxide NPs. The following paragraph will discuss the synthesis of such Ti-based NPs in air and their impact on the mechanical properties of the resulting materials.

New Approach in the Synthesis of Ti-Based NPs and Impact Mechanical Properties. Two photoinitiating systems, namely, TiQ/Iod/EPOX and TiQ/Iod/Trithiol/TMPTA/EPOX, were used to develop, under 385 and 405 nm light exposure, new hybrid organic—inorganic materials containing Ti-based NPs. Evidence suggesting that these particles are attributed to Ti-based NPs synthesized in situ was provided by TEM spectroscopy (Figure 13). Morphological analyses were carried out by TEM spectroscopy to demonstrate the presence of Ti-based nanoparticles produced inside the polymer matrix. The TEM images, reported in Figure 13, show the presence of dispersed spherical Ti-based NPs inside the polymer films with a diameter ranging from 1.8 to 7.3 nm (mean average of 3.5 nm \pm 1.2 nm for the EPOX/TiQ/Iod system) and from 1.8 to 8.2 nm (mean average of 3.7

± 1.9 nm for the EPOX/TMPTA/TiQ/Iod/Trithiol system). No agglomeration of Ti-based NPs was observed, which tantalizingly suggests the polymer matrix to serve as a stabilizing matrix for the photoinduced NPs. Moreover, no Ti-based NPs were observed without the addition of Iod to TiQ. As the thickness of the samples are too high, HAADF-STEM experiments have been performed on both samples to easily observe heavy atoms, which appeared brighter (see Supporting Information Figure S6). The atomic number (Z)contrast results in bright spots corresponding to high Z Tibased nanoparticles in a dark low-Z polymeric matrix. As shown in these micrographs, the photoinduced Ti-based nanoparticles (in white) are mostly well separated and hence contact-free. For example, an optical image of the photosynthesized materials with the TiQ/Iod/Trithiol/TMPTA/ EPOX system is displayed in Figure 13E. This optical image also proves that the Ti-based NPs are well dispersed inside the photoinduced materials as the corresponding material is transparent.

To assess the thermal stability of TiQ/Iod/Trithiol/TMPTA/EPOX nanocomposite, a ramp thermogravimetric

analysis is carried out. The weight loss as a function of temperature is then plotted in Figure 14, which shows that the

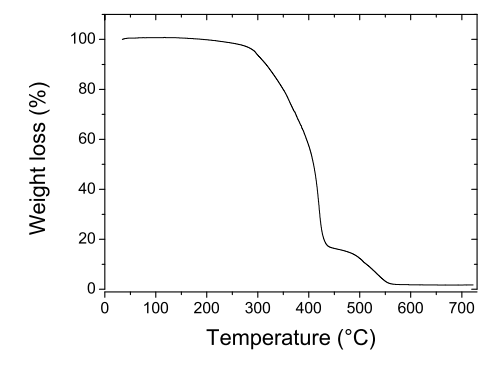


Figure 14. Ramp thermogravimetric analysis obtained for TiQ/Iod/Trithiol/TMPTA/EPOX nanocomposite.

TiQ/Iod/Trithiol/TMPTA/EPOX sample is stable at temperatures up to 300 °C. At this temperature, the material starts to degrade until reaching a pike degradation temperature of 420 °C. At this temperature, more than 80% of the organic mass has been degraded. The remaining mass would correspond to the bulk polymer chains in close interaction with the Ti-based nanoparticles. These chains further degrade at 550 °C, which would be a signature of good interactions between the polymer matrix and the photoinduced Ti-based NPs.

The macroscopic mechanical properties of new EPOX/TMPTA materials based on three different photoinitiating systems (TiQ/Iod/Trithiol, ITX/Iod/Trithiol, and ITX/Iod/Trithiol/TiO₂) were characterized by three-point bending tests. The interest was centered in assessing the influence of the photoinduced Ti-based NPs (from the irradiation of TiQ/Iod/Trithiol photoinitiating system) on the mechanical behavior of the EPOX/TMPTA resin compared to the same resin reticulated under visible light (405 nm), with different photoinitiating systems (ITX/Iod/Trithiol and ITX/Iod/Trithiol/TiO₂). As an example, Figure 15 shows, for each sample, a characteristic flexural stress $\sigma_{\rm f}$ vs flexural strain $\varepsilon_{\rm f}$ plot. The average $\sigma_{\rm f}$ $\varepsilon_{\rm f}$ and flexural modulus $E_{\rm f}$ values obtained from the three-point bending tests are summarized in Table 5.

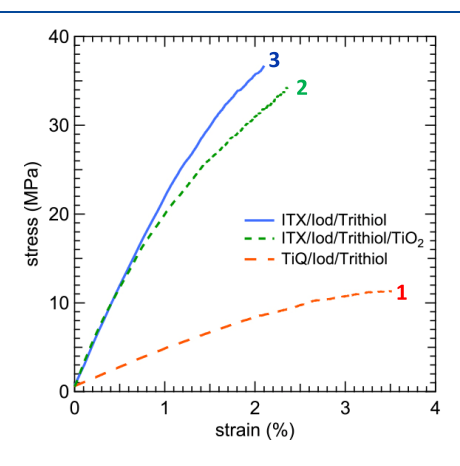


Figure 15. Flexural stress σ_f as a function of the flexural strain ε_f obtained by three-point bending tests for the photoinduced EPOX/TMPTA materials based on (1) TiQ/Iod/Trithiol, (2) ITX/Iod/Trithiol/TiO₂, and (3) ITX/Iod/Trithiol photoinitiating systems.

Table 5. Flexural Modulus E_{\wp} Stress σ_{\wp} and Strain $\varepsilon_{\rm f}$ Obtained by Three-Point Bending Tests for the Photoinduced EPOX/TMPTA Resins Based on (TiQ/Iod/Trithiol), (ITX/Iod/Trithiol), and (ITX/Iod/Trithiol/TiO₂) Photoinitiating Systems

photoinitiating systems	$E_{\rm f}$ (GPa)	$\sigma_{ m f}$ (MPa)	$arepsilon_{ m f}$ (%)
PIS 1: ITX/Iod/Trithiol	1.9	38.7	2.0
PIS 2: $ITX/Iod/Trithiol/TiO_2$	1.7	39.2	2.5
PIS 3: TiQ/Iod/Trithiol	0.4	9.7	3.4

First, it is seen that the mechanical values listed in Table 5 agree very well with prototypical epoxy resins reported in the literature. 42-44 Furthermore, the neat photosensitized EPOX/ TMPTA resin containing ITX/Iod/Trithiol (PIS 1) as a photoinitiating system was compared to the same one but with the introduction of TiO₂ nanoparticles (PIS 2). Both materials are synthesized to compare their mechanical properties to those of the TiQ-based material (PIS 3), thus demonstrating the positive influence of the photoinduced generation of Tibased NPs (from TiQ/Iod/Trithiol photoinitiating system, PIS 3) under visible light irradiation. It can be seen in both Figure 15 and Table 5 that the presence of TiO₂ NPs (PIS 2) globally induces a drop on the flexural modulus $E_{\rm f}$ stress $\sigma_{\rm f}$ and strain ε_f . This would mean that the sole presence of TiO₂. NPs in this case yields a fragile material exhibiting a loss in the mechanical properties and clearly evidences the weak dispersion of TiO₂ NPs in the polymer matrix. This contrasts with the results obtained for TiQ because our system also induces a drop on the flexural modulus E_f and flexural stress σ_f but yet increases the maximum strain ε_{θ} compared to the neat EPOX/TMPTA resin containing ITX/Iod/Trithiol (PIS 1) or ITX/Iod//Trithiol/TiO₂ NPs (PIS 2). This would mean that the nanocomposite containing TiQ (and Ti-based NPs) is tougher (i.e., less fragile) material compared to the former two materials containing either ITX/Iod/Trithiol (PIS 1) or ITX/ Iod/Trithiol/TiO₂ (PIS 2) as a photoinitiating system. In conclusion, the photogeneration of Ti-based NPs (from the TiQ/Iod/Trithiol photoinitiating system) in the polymer matrix leads to an increase of its mechanical resistance by toughening the matrix.

CONCLUSIONS

A well-performing photoinitiating system based on a welldefined titanium precursor complex that derives from the ringopening and coupling of two quinoline molecules was reported in this study (TiQ). This system performs both free-radical and cationic photopolymerizations of TMPTA and EPOX, respectively, under visible light irradiation along with the formation of Ti-based nanoparticles (NPs). The use of a quinoline-derived titanium complex TiQ in combination with an iodonium salt (Iod) as an efficient visible light photoinitiating system is an unprecedented combination for overcoming the oxygen inhibition in free-radical photopolymerization under air. The TiQ/Iod photoinitiating system was also found to promote efficiently, and in a one-step process, an interpenetrated network in the radical and cationic photopolymerizations of an epoxide/acrylate blend upon LED@405 nm. Interestingly, our studies reveal that the conditions used for TiQ/Iod PIs lead to the generation of Tibased NPs under visible light irradiation inside the polymerized coatings. The macroscopic mechanical properties of the resulting TiQ-based nanocomposite also result in the

generation of these Ti-based NPs within the polymer matrix, which in turn results in an increase of its mechanical resistance by toughening the matrix. These unprecedented results might open the gate for the synthesis of newly hybrid materials using well-defined early-transition metal complexes.

ASSOCIATED CONTENT

S Supporting Information

The Supporting Information is available free of charge on the ACS Publications website at DOI: 10.1021/acs.macromol.8b02719.

All of the kinetics profiles for the free-radical polymerization of TMPTA with ITX/Trithiol, ITX/MDEA, and TiQ/Iod/Trithiol photoinitiatings systems upon LEDs@385 and 405 nm irradiation (under air and in laminate conditions) (Figures S1-S3); decay traces of TiQ triplet state (3TiQ) at 440 nm after a laser pulse (λ_{ex} = 385 nm) of argon (1) and O₂ (2)—saturated toluene solution of TiQ (Figure S4); cyclic voltammetry of TiQ in ["Bu₄N][PF₆]/THF (0.2 M electrolyte, room temperature, under N₂ (Figure S5); and HAADF-STEM images of Ti NPs inside coatings from (A) TiQ/Iod/ EPOX system upon an LED@385 nm exposure (44 mW/cm2 under air and (B) EPOX/TMPTA blend (50/50%, w/w) in the presence of TiQ/Iod/Trithiol upon an LED@405 nm exposure (100 mW/cm²) under air, irradiation time = 800 s (Figure S6) (PDF)

AUTHOR INFORMATION

Corresponding Author

*E-mail: versace@icmpe.cnrs.fr.

ORCID ®

Agustin Rios de Anda: 0000-0003-3497-9483 Takashi Kurogi: 0000-0002-8804-757X Daniel J. Mindiola: 0000-0001-8205-7868 Davy-Louis Versace: 0000-0002-4272-5021

Author Contributions

The manuscript was written through contributions of all authors. All authors have given approval to the final version of the manuscript. The authors contributed equally.

Notes

The authors declare no competing financial interest.

ACKNOWLEDGMENTS

This work was supported by the Slovak Research and Development Agency under the contract No. APVV-15-0053. Vlasta Brezová acknowledges Ministry of Education, Science, Research and Sport of the Slovak Republic, for funding within the scheme "Excellent research teams". D.J.M. acknowledges the US National Science Foundation (CHE-0848248 and CHE-1152123) and the University of Pennsylvania for financial support of this research. T.K. acknowledges financial support from the JSPS (Japan Society for the Promotion of Science) for a postdoctoral fellowship. Dr. Davy-Louis Versace acknowledges French National Research Agency (ANR), UPEC, and ICMPE for financial support.

■ REFERENCES

(1) Vitale, A.; Sangermano, M.; Bongiovanni, R.; Burtscher, P.; Moszner, N. Visible Light Curable Restorative Composites for Dental Applications Based on Epoxy Monomer. *Materials* **2014**, *7*, 554–562.

(2) Jeon, I.-Y.; Baek, J.-B. Nanocomposites Derived from Polymers and Inorganic Nanoparticles. *Materials* **2010**, *3*, 3654–3674.

- (3) Kim, J.-J.; Moon, H.-J.; Lim, B.-S.; Lee, Y.-K.; Rhee, S.-H.; Yang, H.-C. The Effect of Nanofiller on the Opacity of Experimental Composites. J. Biomed. Mater. Res., Part B 2007, 80, 332–338.
- (4) Salgado, V. E.; Borba, M. M.; Cavalcante, L. M.; de Moraes, R. R.; Schneider, L. F. Effect of Photoinitiator Combinations on Hardness, Depth of Cure, and Color of Model Resin Composites. *J. Esthet. Restor. Dent.* **2015**, 27, S41–S48.
- (5) Salgado, V. E.; Cavalcante, L. M.; Silikas, N.; Schneider, L. F. J. The influence of nanoscale inorganic content over optical and surface properties of model composites. *J. Dent.* **2013**, *41*, No. e45.
- (6) Antonucci, J.; Dickens, S. Base and Diluent Monomers. *Biomaterials Science*, 3rd ed.; Ratner, B. D., Hoffman, A. S., Schoen, F. J., Lemons, J. E., Eds.; Academic Press, 2013.
- (7) Fink, J. K. Acrylic Dental Fillers. *Reactive Polymers Fundamentals and Applications*, 2nd ed.; Fink, J. K., Ed.; William Andrew Publishing: Oxford, 2013; Chapter 19, pp 453–474.
- (8) Antonucci, J.; Dickens, S. D Acrylics. *Biomaterials Science*, 3rd ed.; Ratner, B. D., Hoffman, A. S., Schoen, F. J., Lemons, J. E., Eds.; Academic Press, 2013; pp 103–111.
- (9) Xu, H. H. K.; Cheng, L.; Zhang, K.; Melo, M. A. S.; Weir, M. D.; Antonucci, J. M.; Lin, N. J.; Lin-Gibson, S.; Chow, L. C.; Zhou, X. Nanostructured Dental Composites and Adhesives with Antibacterial and Remineralizing Capabilities for Caries Inhibition. *Nanobiomaterials in Clinical Dentistry*; Subramani, K., Ahmed, W., Hartsfield, J. K., Eds.; William Andrew Publishing, 2013; Chapter 6, pp 109–129.
- (10) Abou Neel, E. A.; Young, A. M. Antibacterial adhesives for bone and tooth repair. In *Joining and Assembly of Medical Materials and Devices*; Zhou, Y., Breyen, M. D., Eds.; Woodhead Publishing, 2013; Chapter 17, pp 491–513.
- (11) McGilvray, K. L.; Decan, M. R.; Wang, D.; Scaiano, J. C. Facile Photochemical Synthesis of Unprotected Aqueous Gold Nanoparticles. *J. Am. Chem. Soc.* **2006**, *128*, 15980–15981.
- (12) Scaiano, J. C.; Billone, P.; Gonzalez, C. M.; Maretti, L.; Marin, M. L.; McGilvray, K. L.; Yuan, N. Photochemical routes to silver and gold nanoparticles. *Pure Appl. Chem.* **2009**, *81*, 635–647.
- (13) Stamplecoskie, K. G.; Scaiano, J. C. Silver as an Example of the Applications of Photochemistry to the Synthesis and Uses of Nanomaterials. *Photochem. Photobiol.* **2012**, *88*, 762–768.
- (14) Marin, M. L.; McGilvray, K. L.; Scaiano, J. C. Photochemical Strategies for the Synthesis of Gold Nanoparticles from Au(III) and Au(I) Using Photoinduced Free Radical Generation. *J. Am. Chem. Soc.* **2008**, *130*, 16572–16584.
- (15) Stamplecoskie, K. G.; Scaiano, J. C. Kinetics of the Formation of Silver Dimers: Early Stages in the Formation of Silver Nanoparticles. *J. Am. Chem. Soc.* **2011**, *133*, 3913–3920.
- (16) Liu, Z.; Cao, Z.; Deng, B.; Wang, Y.; Shao, J.; Kumar, P.; Liu, C. R.; Wei, B.; Cheng, G. J. Ultrafast and scalable laser liquid synthesis of tin oxide nanotubes and its application in lithium ion batteries. *Nanoscale* **2014**, *6*, 5853–5858.
- (17) Scaiano, J. C.; Stamplecoskie, K. G.; Hallett-Tapley, G. L. Photochemical Norrish type I reaction as a tool for metal nanoparticle synthesis: importance of proton coupled electron transfer. *Chem. Commun.* **2012**, *48*, 4798–4808.
- (18) Fouassier, J. P.; Lalevée, J. Photoinitiators for Polymer Synthesis: Scope, Reactivity and Efficiency; Wiley-VCH Verlag GmbH & Co. KGaA: Weinheim, 2012.
- (19) Souane, R.; Tehfe, M. A.; Lalevée, J.; Gigmes, D.; Fouassier, J. P. New Initiating Systems for Thermal Cationic Polymerization at Ambient Temperature with in situ Formation of Ag(0) Nanoparticles: A Silane/Silver Salt Combination. *Macromol. Chem. Phys.* **2010**, *211*, 1441–1445.
- (20) Balan, L.; Malval, J.-P.; Schneider, R.; Le Nouen, D.; Lougnot, D.-J. In-situ fabrication of polyacrylate-silver nanocomposite through photoinduced tandem reactions involving eosin dye. *Polymer* **2010**, *51*, 1363–1369.

(21) Malval, J.-P.; Jin, M.; Balan, L.; Schneider, R.; Versace, D.-L.; Chaumeil, H. ln; Defoin, A.; Soppera, O. *J. Phys. Chem. C* **2010**, *114*, 10396–10402.

- (22) Nehlig, E.; Schneider, R.; Vidal, L.; Clavier, G.; Balan, L. Silver Nanoparticles Coated with Thioxanthone Derivative as Hybrid Photoinitiating Systems for Free Radical Polymerization. *Langmuir* **2012**, 28, 17795–17802.
- (23) Anyaogu, K. C.; Cai, X.; Neckers, C. Macromolecules 2008, 41, 9000-9003.
- (24) Mokbel, H.; Dumur, F.; Telitel, S.; Vidal, L.; Xiao, P.; Versace, D.-L.; Tehfe, M.-A.; Morlet-Savary, F.; Graff, B.; Fouassier, J.-P.; Gigmes, D.; Toufaily, J.; Hamieh, T.; Lalevee, J. Photoinitiating systems of polymerization and in situ incorporation of metal nanoparticles into polymer matrices upon exposure to visible light: push—pull malonate and malononitrile based dyes. *Polym. Chem.* **2013**, *4*, 5679—5687.
- (25) Yagci, Y.; Sangermano, M.; Rizza, G. In situ synthesis of gold-cross-linked poly(ethylene glycol) nanocomposites by photoinduced electron transfer and free radical polymerization processes. *Chem. Commun.* **2008**, *0*, 2771–2773.
- (26) Sangermano, M.; Yagci, Y.; Rizza, G. In Situ Synthesis of Silver–Epoxy Nanocomposites by Photoinduced Electron Transfer and Cationic Polymerization Processes. *Macromolecules* **2007**, *40*, 8827–8829.
- (27) Yagci, Y.; Sangermano, M.; Rizza, G. A visible light photochemical route to silver–epoxy nanocomposites by simultaneous polymerization–reduction approach. *Polymer* **2008**, *49*, 5195–5198.
- (28) Malval, J.-P.; Jin, M.; Balan, L.; Schneider, R.; Versace, D.-L.; Chaumeil, H.; Defoin, A.; Soppera, O. Photoinduced Size-Controlled Generation of Silver Nanoparticles Coated with Carboxylate-Derivatized Thioxanthones. *J. Phys. Chem. C* **2010**, *114*, 10396–10402.
- (29) Sautrot-Ba, P.; Bogliotti, N.; Brosseau, A.; Bourgon, J.; Mazeran, P.-E.; Lalevée, J.; Morlet-Savary, F.; Versace, D.-L. A (triphenylphosphine)Silver (I) complex as a new performance additive for simultaneously promoting the Synthesis of Nanoparticles under air and overcoming Oxygen Inhibition Effects. *Macromol. Mater. Eng.* **2018**, *303*, No. 1800101.
- (30) Versace, D.-L.; Cerezo Bastida, J.; Lorenzini, C.; Cachet-Vivier, C.; Renard, E.; Langlois, V.; Malval, J.-P.; Fouassier, J.-P.; Lalevée, J. A Tris(triphenylphosphine)ruthenium(II) Complex as a UV Photoinitiator for Free-Radical Polymerization and in Situ Silver Nanoparticle Formation in Cationic Films. *Macromolecules* **2013**, *46*, 8808–8815
- (31) Balan, L.; Jin, M.; Malval, J.-P.; Chaumeil, H. In; Defoin, A.; Vidal, L. Fabrication of Silver Nanoparticle-Embedded Polymer Promoted by Combined Photochemical Properties of a 2,7-Diaminofluorene Derivative Dye. *Macromolecules* **2008**, *41*, 9359–9365.
- (32) Versace, D.-L.; Fouassier, J.-P.; Lalevée, J. The First Photochemical In Situ Production of Ti-Based Nanoparticles: A SH2 Strategy Using Bis(cyclopentadienyl)titanium Dichloride (Cp2TiCl2). Macromol. Rapid Commun. 2014, 35, 821–826.
- (33) Versace, D.-L.; Dalmas, F.; Fouassier, J.-P.; Lalevee, J. Zirconocene Dichloride: An Efficient Cleavable Photoinitiator Allowing the in Situ Production of Zr-Based Nanoparticles Under Air. ACS Macro Lett. **2013**, *2*, 341–345.
- (34) Lalevée, J.; Bourgon, J.; Poupart, R.; Leroy, E.; Cerezo Batisda, J.; Fouassier, J.-P.; Versace, D.-L. Oxygen-Mediated Reactions in Photopolymerizable Radical Thin Films: Application to Simultaneous Photocuring Under Air and Nanoparticle Formation. *Macromol. Chem. Phys.* **2015**, 216, 1702–1711.
- (35) Lalevée, J.; Poupart, R.; Bourgon, J.; Fouassier, J. P.; Versace, D. L. In situ production of visible light absorbing Ti-based nanoparticles in solution and in a photopolymerizable cationic matrix. *Chem. Commun.* **2015**, *51*, 5762–5765.
- (36) Baek, S.-Y.; Kurogi, T.; Kang, D.; Kamitani, M.; Kwon, S.; Solowey, D. P.; Chen, C.-H.; Pink, M.; Carroll, P. J.; Mindiola, D. J.;

Baik, M.-H. Room Temperature Ring-Opening of Quinoline, Isoquinoline and Pyridine with Low-Valent Titanium. *J. Am. Chem. Soc.* **2017**, *139*, 12804–12814.

- (37) Duling, D. R. Simulation of Multiple Isotropic Spin-Trap EPR Spectra. J. Magn. Reson., Ser. B 1994, 104, 105–110.
- (38) Stoll, S.; Schweiger, A. EasySpin, a comprehensive software package for spectral simulation and analysis in EPR. *J. Magn. Reson.* **2006**, *178*, 42–55.
- (39) Bonneau, R.; Carmichael, I.; Hug, G. L. Molar absorption coefficients of transient species in solution. *Pure Appl. Chem.* **1991**, *63*, 289–299.
- (40) Rehm, D.; Weller, A. Kinetics of Fluorescence Quenching by Electron and H-Atom Transfer. *Isr. J. Chem.* **1970**, *8*, 259–271.
- (41) Gontard, L. C.; Ozkaya, D.; Dunin-Borkowski, R. E. A simple algorithm for measuring particle size distributions on an uneven background from TEM images. *Ultramicroscopy* **2011**, *111*, 101–106.
- (42) Kothmann, M. K.; Ziadeh, M.; Bakis, G.; Rios de Anda, A.; Breu, J.; Altstädt, V. Analyzing the influence of particle size and stiffness state of the nanofiller on the mechanical properties of epoxy/clay nanocomposites using a novel shear-stiff nano-mica. *J. Mater. Sci.* **2015**, *50*, 4845–4859.
- (43) Kothmann, M. H.; Zeiler, R.; Rios de Anda, A.; Brückner, A.; Altstädt, V. Fatigue crack propagation behaviour of epoxy resins modified with silica-nanoparticles. *Polymer* **2015**, *60*, 157–163.
- (44) Utaloff, K.; Kothmann, M. H.; Ciesielski, M.; Döring, M.; Neumeyer, T.; Altstädt, V.; Gorman, I.; Henningsen, M. Improvement of fracture toughness and glass transition temperature of DGEBA-based epoxy systems using toughening and crosslinking modifiers. *Polym. Eng. Sci.* **2019**, *59*, 86–95.
- (45) Sales, E. S.; Schneider, J. M. F. M.; Santos, M. J. L.; Bortoluzzi, A. J.; Cardoso, D. R.; Santos, W. G.; Merlo, A. A. Quinolines by Three-Component Reaction: Synthesis and Photophysical Studies. *J. Braz. Chem. Soc.* **2015**, *26*, 562–571.
- (46) Condat, M.; Mazeran, P. E.; Malval, J. P.; Lalevée, J.; Morlet-Savary, F.; Renard, E.; Langlois, V.; Abbad Andalloussi, S.; Versace, D. L. Photoinduced curcumin derivative-coatings with antibacterial properties. *RSC Adv.* **2015**, *5*, 85214–85224.
- (47) Jin, M.; Xie, J.; Malval, J.-P.; Spangenberg, A.; Soppera, O.; Versace, D.-L.; Leclerc, T.; Pan, H.; Wan, D.; Pu, H.; Baldeck, P.; Poizat, O.; Knopf, S. Two-photon lithography in visible and NIR ranges using multibranched-based sensitizers for efficient acid generation. J. Mater. Chem. C 2014, 2, 7201–7215.
- (48) Peter Pappas, S.; Pappas, B. C.; Gatechair, L. R.; Jilek, J. H.; Schnabel, W. Photoinitiation of Cationic Polymerization. IV. Direct and Sensitized Photolysis of Aryl lodonium and Sulfonium Salts. *Polym. Photochem.* **1984**, *5*, 1–22.
- (49) Peter Pappas, S.; Pappas, B. C.; Gatechair, L. R.; Schnabel, W. Photoinitation of Cationic Polymerization. II. Laser Flash Photolysis of Diphenyliodonium Salts. *J. Polym. Sci.: Polym. Chem. Ed.* **1984**, 22, 69–76.
- (50) Pappas, S. P. Photoinitiated Cationic Polymerization. In *Photopolymerisation and Photoimaging Science and Technology*; Allen, N. S., Ed.; Springer: Dordrecht, 1989; pp 55–73.
- (51) Amirzadeh, G.; Schnabel, W. On the photoinitiation of free radical polymerization-laser flash photolysis investigations on thioxanthone derivatives. *Makromol. Chem.* 1981, 182, 2821–2835.
- (52) Allen, N. S.; Catalina, F.; Peinado, C.; Sastre, R.; Mateo, J. L.; Green, P. N. Synthesis, characterization and photopolymerization activity of a novel thioxanthone monomer and photopolymers. *Eur. Polym. J.* **1987**, 23, 985–987.
- (53) Yates, S. F.; Schuster, G. B. Photoreduction of triplet thioxanthone by amines: charge transfer generates radicals that initiate polymerization of olefins. *J. Org. Chem.* **1984**, *49*, 3349–3356.
- (54) Davidson, R. S., Photochemical Reactions Involving Charge-Transfer Complexes. In *Molecular Association*, Foster, R., Ed.; Academic Press: New York, 1975; Vol. 1, pp 215–334.
- (55) Cokbaglan, L.; Arsu, N.; Yagci, Y.; Jockusch, S.; Turro, N. J. 2-Mercaptothioxanthone as a Novel Photoinitiator for Free Radical Polymerization. *Macromolecules* **2003**, *36*, 2649–2653.

(56) Cramer, N. B.; Bowman, C. N. Kinetics of thiol—ene and thiol—acrylate photopolymerizations with real-time fourier transform infrared. *J. Polym. Sci. Part A: Polym. Chem.* **2001**, *39*, 3311–3319.

- (57) Dénès, F.; Pichowicz, M.; Povie, G.; Renaud, P. Thiyl Radicals in Organic Synthesis. *Chem. Rev.* **2014**, *114*, 2587–2693.
- (58) O'Brien, A. K.; Cramer, N. B.; Bowman, C. N. Oxygen inhibition in thiol—acrylate photopolymerizations. *J. Polym. Sci. Part A: Polym. Chem.* **2006**, *44*, 2007–2014.
- (59) Lalevée, J.; Allonas, X.; Fouassier, J.-P. Reactivity of Carbon-Centered Radicals toward Acrylate Double Bonds: Relative Contribution of Polar vs Enthalpy Effects. J. Phys. Chem. A 2004, 108, 4326–4334.
- (60) Fouassier, J. P.; Lalevée, J. Photochemical Production of Interpenetrating Polymer Networks; Simultaneous Initiation of Radical and Cationic Polymerization Reactions. *Polymers* **2014**, *6*, 2588–2610.
- (61) Jockusch, S.; Turro, N. J. Radical Addition Rate Constants to Acrylates and Oxygen: R-Hydroxy and R-Amino Radicals Produced by Photolysis of Photoinitiators. *J. Am. Chem. Soc.* **1999**, *121*, 3921–3925.
- (62) Xiao, P.; Dumur, F.; Graff, B.; Morlet-Savary, F.; Vidal, L.; Gigmes, D.; Fouassier, J. P.; Lalevée, J. Structural Effects in the Indanedione Skeleton for the Design of Low Intensity 300–500 nm Light Sensitive Initiators. *Macromolecules* **2014**, *47*, 26–34.
- (63) Xiao, P.; Dumur, F.; Graff, B.; Fouassier, J. P.; Gigmes, D.; Lalevée, J. Cationic and Thiol—Ene Photopolymerization upon Red Lights Using Anthraquinone Derivatives as Photoinitiators. *Macromolecules* **2013**, *46*, 6744–6750.
- (64) Zivic, N.; Zhang, J.; Bardelang, D.; Dumur, F.; Xiao, P.; Jet, T.; Versace, D.-L; Dietlin, C.; Morlet-Savary, F.; Graff, B.; Fouassier, J.-P.; Gigmes, D.; Lalevée, J. Novel naphthalimide-amine based photo-initiators operating under violet and blue LEDs and usable for various polymerization reactions and synthesis of hydrogels. *Polym.Chem.* **2016**, *7*, 418–429.
- (65) Al Mousawi, A.; Kermagoret, A.; Versace, D.-L.; Toufaily, J.; Hamieh, T.; Graff, B.; Dumur, F.; Gigmes, D.; Fouassier, J. P.; Lalevée, J. Copper photoredox catalysts for polymerization upon near UV or visible light: structure/reactivity/efficiency relationships and use in LED projector 3D printing resins. *Polym. Chem.* **2017**, *8*, 568–580.
- (66) Devoe, R. J.; Sahyun, M. R. V.; Serpone, N.; Sharma, D. K. Transient intermediates in the photolysis of iodonium cations. *Can. J. Chem.* **1987**, *65*, 2342–2349.
- (67) Buettner, G. R. Spin Trapping: ESR parameters of spin adducts 1474 1528V. Free Radic. Biol. Med. 1987, 3, 259–303.
- (68) Jones, C. M.; Burkitt, M. J. EPR detection of the unstable tert-butylperoxyl radical adduct of the spin trap 5,5-dimethyl-1-pyrroline N-oxide: a combined spin-trapping and continuous-flow investigation. *J. Chem. Soc., Perkin Trans.* 2 2002, 12, 2044–2051.
- (69) Sato, T.; Hamada, Y.; Sumikawa, M.; Araki, S.; Yamamoto, H. Solubility of Oxygen in Organic Solvents and Calculation of the Hansen Solubility Parameters of Oxygen. *Ind. Eng. Chem. Res.* **2014**, 53, 19331–19337.
- (70) Berti, C.; Colonna, M.; Greci, L.; Marchetti, L. Stable nitroxide radicals from 2-substituted quinoline-N-oxides with organometallic compounds. *Tetrahedron* **1976**, 32, 2147–2151.
- (71) Atmaram, S.; Forrester, A. R.; Gill, M.; Napier, R. J.; Thomson, R. H. Intramolecular cyclisation of iminoxyl radicals. *Acta Chem. Scand., Ser. B* **1982**, *36*, 641–647.
- (72) Yao, M.; Shibuya, H.; Kato, T.; Inoue, H.; Yoshioka, N. Synthesis and magnetic properties of 2,2,4- and 2,2,6-triphenyl-1,2-dihydroquinoline-N-oxyl derivatives. *Polyhedron* **2005**, 24, 2828–2834.
- (73) Lion, Y.; Gandin, E.; Van de Vorst, A. On the production of nitroxide radicals by singlet oxygen reaction: an EPR study. *Photochem. Photobiol.* **1980**, *31*, 305–309.
- (74) Wu, H.; Song, Q.; Ran, G.; Lu, X.; Xu, B. Recent developments in the detection of singlet oxygen with molecular spectroscopic methods. *TrAC Trends Anal. Chem.* **2011**, *30*, 133–141.

(75) Dvoranová, D.; Barbieriková, Z.; Brezová, V. Radical Intermediates in Photoinduced Reactions on TiO2 (An EPR Spin Trapping Study). *Molecules* **2014**, *19*, 17279–17304.